

## Momentum-Resolved Electron-Phonon Interaction in Lead Determined by Neutron Resonance Spin-Echo Spectroscopy

T. Keller,<sup>1,2</sup> P. Aynajian,<sup>1</sup> K. Habicht,<sup>3</sup> L. Boeri,<sup>1</sup> S. K. Bose,<sup>4</sup> and B. Keimer<sup>1</sup>

<sup>1</sup>Max-Planck-Institut für Festkörperforschung, Heisenbergstrasse 1, D-70569 Stuttgart, Germany

<sup>2</sup>ZWE FRMII, Technical University of Munich, Lichtenbergstrasse 1, D-85748 Garching, Germany

<sup>3</sup>Hahn-Meitner-Institut, Glienicker Strasse 100, D-14109 Berlin, Germany

<sup>4</sup>Brock University, 500 Glenridge Avenue, St. Catharines, Ontario L2S 3A1, Canada

(Received 26 January 2006; revised manuscript received 15 March 2006; published 5 June 2006)

Neutron resonance spin-echo spectroscopy was used to monitor the temperature evolution of the linewidths of transverse acoustic phonons in lead across the superconducting transition temperature  $T_c$  over an extended range of the Brillouin zone. For phonons with energies below the superconducting energy gap, a linewidth reduction of maximum amplitude  $\sim 6 \mu\text{eV}$  was observed below  $T_c$ . The electron-phonon contribution to the phonon lifetime extracted from these data is in satisfactory overall agreement with *ab initio* lattice-dynamical calculations, but significant deviations are found.

DOI: [10.1103/PhysRevLett.96.225501](https://doi.org/10.1103/PhysRevLett.96.225501)

PACS numbers: 63.20.Kr, 61.12.Ex, 74.25.Kc, 74.70.Ad

The electron-phonon interaction is the major limiting factor for electronic transport phenomena in metals at elevated temperatures, and it is responsible for most instances of superconductivity. For metallic and superconducting elements [1] and binary compounds such as  $\text{MgB}_2$  [2], modern *ab initio* calculations yield accurate predictions for the electron-phonon coupling parameters of every phonon over the entire Brillouin zone (BZ). An active area of research is aimed at a realistic description of electron-lattice interactions in complex compounds with strong electronic correlations. Yet only rudimentary experimental tests of these calculations have thus far proven possible. For instance, electronic transport or tunneling experiments probe weighted averages of the electron-phonon interaction over the entire phonon spectrum. Optical spectroscopy is capable of probing the lifetimes of individual phonons limited by scattering from electrons, but kinematics constrains these experiments to a single point in momentum space. Here we use a new neutron spectroscopy method with an energy resolution in the  $\mu\text{eV}$  range (that is, about 2 orders of magnitude better than that of standard neutron spectroscopy) to determine the electron-phonon lifetime of an individual acoustic phonon in lead over an extended range of the BZ. The results are compared to *ab initio* lattice-dynamical calculations also reported here. Our experiment constitutes the first detailed test of modern calculations of the electron-phonon interaction and opens up a new avenue for a quantitative understanding of electron-phonon interactions and superconductivity in solids.

Since the 1950s, triple-axis spectrometry (TAS) with neutrons (and, recently, x rays) has been the method of choice to experimentally determine the energy- and momentum-resolved phonon spectra of solids. Briefly, the energies and momenta of the incoming and scattered neutrons are selected by crystal monochromators, and their difference yields the phonon dispersion relation. The monochromaticity of the beam is thus coupled to the

beam divergence, which can be restricted only at the expense of beam intensity. This implies that energy resolutions significantly better than 10% are impractical to achieve under almost all circumstances. Since the electron-phonon interaction leads to a phonon linewidth broadening of typically less than 1%, TAS allows phonon lifetime measurements only in exceptional cases. While the phonon dispersions in lead were determined by TAS early on [3], attempts to resolve the electron-phonon lifetimes have been unsuccessful [4,5]. TAS is therefore not generally applicable as a probe of the electron-phonon interaction in metals.

A neutron spin-echo method to improve the energy resolution of TAS by several orders of magnitude without loss of intensity was proposed some time ago [6]. The method has been described in detail elsewhere [7]. Briefly, it is implemented by inserting spin polarizers and tunable Larmor precession coils into the incident and scattered beams of the triple-axis spectrometer. If the phonon to be measured has an infinite lifetime, and if the precession fields are properly matched (spin-echo condition), the full polarization of the incident beam is recovered at the detector. If the phonon lifetime is finite, the spin-echo amplitude is reduced, and the phonon linewidth can be determined by systematically varying the precession fields. Early versions of this technique have enabled the determination of the lifetimes of rotons in superfluid helium [8] and optical phonons near the BZ boundary in germanium [9]. However, a major technical obstacle has thus far prevented more general applications. The dispersive nature of most collective excitations in solids leads to a degradation of the neutron spin polarization that masks the effect of the finite excitation lifetime. This effect can be compensated to linear order by tilting the precession coils away from the neutron beam direction by an angle proportional to the slope of the dispersion relation [7]. Since the required tilt angles are of order  $10^\circ$ – $50^\circ$ , however, this

cannot be accomplished by the long solenoids used in the early work.

In the “neutron resonance spin-echo” (NRSE) technique [7,10], the solenoids are replaced by a pair of compact radio-frequency (rf) coils surrounding a field-free region. This allows larger tilt angles sufficient to match the dispersion relations of most collective excitations in solids. Using a prototype NRSE-TAS setup, the feasibility of phonon lifetime measurements in lead was demonstrated at temperatures exceeding 50 K, where the lifetime is limited by phonon anharmonicity [11]. However, the neutron flux was insufficient to obtain high-quality data at lower temperatures, where the electron-phonon interaction is dominant.

Here we report the results of experiments carried out at the dedicated, high-flux NRSE-TAS spectrometer TRISP at the FRM-II neutron source in Garching, Germany [12]. Starting from the source, in-beam components include: a spin-polarizing guide; a velocity selector to cut out higher-order contamination of the incident beam; a horizontally and vertically focusing pyrolytic-graphite (PG) monochromator and a horizontally focusing PG analyzer, each set for the (002) reflection; and a supermirror spin polarizer in front of the detector. The measurements closely followed the protocol established in Ref. [11]. The reader is advised to consult this reference for a detailed description of the experimental setup and data analysis. The samples were two cylindrical Pb single crystals with cylinder axes (100) and (110) and mosaicities  $4.2^\circ$  and  $5.7^\circ$ , respectively. Both crystals had a diameter of 30 mm and a length of 50 mm. The first crystal was used to measure the  $T_1$  phonon along (110) and the  $T$  phonon along (100) in the scattering plane spanned by the (001) and (010) directions of the reciprocal lattice. The remaining measurements were carried out with the second sample. The samples were loaded into a closed-cycle He cryostat. Depending on phonon energy, the incident (final) neutron wave vector was fixed at  $2.51 \text{ \AA}^{-1}$  ( $1.7 \text{ \AA}^{-1}$ ). The triple-axis spectrometer was aligned in a defocusing configuration in order to minimize the segment of the dispersion surface sampled by the TAS resolution ellipsoid. The spectrometer angles were tuned to maximize the phonon intensity and kept constant during the spin-echo scans. The NRSE coils between monochromator and sample and between sample and analyzer were tilted to match the slope of the acoustic phonon dispersions. The spin-echo time  $\tau$  was changed by varying the rf frequencies in the NRSE coils. In order to minimize systematic errors, the beam polarization at the detector  $P$  was determined by translating the coil immediately in front of the detector and extracting the amplitude of the resulting sinusoidal intensity modulation from a least-squares fit [11].

The strategy of the experiment was to single out the electron-phonon contribution to the phonon lifetime by monitoring the evolution of the phonon line shape through the superconducting transition temperature  $T_c = 7.2 \text{ K}$ . As

demonstrated previously by TAS for phonons with anomalously large linewidths in  $\text{Nb}_3\text{Sn}$  [13] and Nb [14], this contribution vanishes if the phonon energy is below the superconducting energy gap  $2\Delta$ . Other intrinsic contributions to the phonon linewidth, such as isotope disorder and the anharmonicity of the lattice potential, do not exhibit anomalies at  $T_c$ .

Because of its face-centered cubic lattice structure, the phonon spectrum of lead consists entirely of acoustic branches. Most of the data were taken on the lowest-lying transverse mode  $T_1$  in the  $(\xi\xi 0)$  direction, where all phonons are nondegenerate. The atomic displacements of this mode are along  $(1\bar{1}0)$ . The mode energy is lower than  $2\Delta$  over much of the BZ, so that a large range of phonon momenta can be covered in this way. More limited data sets were also acquired for the  $T_2$  mode [with displacements in the (001) direction] along  $(\xi\xi 0)$  and for the transverse phonon along  $(\xi\xi\xi)$ .

Figure 1 shows typical NRSE data for the  $T_1$  mode along  $(\xi\xi 0)$ . The dependence of the beam polarization on the spin-echo time  $P(\tau)$  is proportional to the Fourier transform of the phonon line shape [7]. As a Lorentzian line shape thus yields an exponential NRSE profile, the phonon linewidth can be obtained from the slope  $\Gamma$  of  $P(\tau)$  on a semilogarithmic plot (lines in Fig. 1). A drop of the slope (corresponding to an increase of the phonon lifetime) below  $T_c$  is clearly apparent. In addition to the intrinsic phonon linewidth,  $\Gamma$  is also affected by extrinsic factors such as the mosaicity of the crystal and the curvature of the dispersion relation, as discussed in detail in Refs. [11,15]. However, these temperature-independent factors have a negligible influence on the linewidth anomaly at  $T_c$ , which is of interest here. A detailed discussion of resolution effects on the present data will thus be given elsewhere

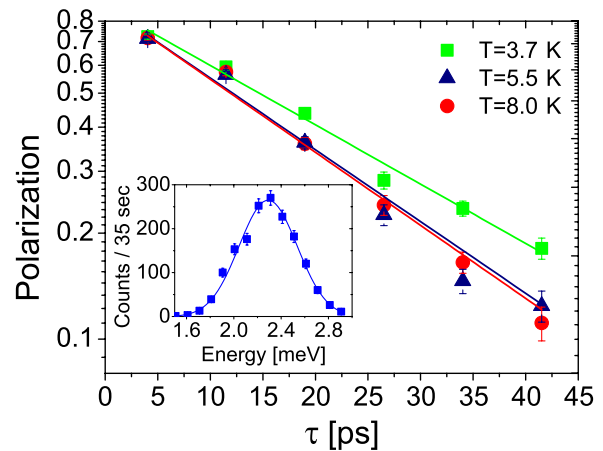


FIG. 1 (color online). Neutron resonance spin-echo profiles for the  $T_1$  phonon at  $(0.3, 0.3, 0)$  at selected temperatures above and below the superconducting transition temperature. The inset shows a triple-axis scan in focusing mode for the same phonon. From these data,  $\Gamma$  was extracted as  $25.5 \pm 0.6$ ,  $31.4 \pm 0.8$ , and  $30.9 \pm 0.7 \mu\text{eV}$  for  $T = 3.7, 5.5,$  and  $8.0 \text{ K}$ , respectively.

[16]. In the following figures presenting the experimentally observed  $\Gamma$  versus temperature, the extraneous contributions give rise to zero-temperature offsets that generally decrease with increasing wave vector, due to the decreasing curvature of the dispersion surface sampled by the TAS resolution volume.

Figures 2(a)–2(e) shows the temperature dependence of  $\Gamma$  for selected  $T_1$  phonons along  $(\xi\xi0)$ . A decrease of  $\Gamma$  at  $T_c$  is evident in all of the traces shown for  $\xi \leq 0.32$  ( $E \leq 2.46$  meV). The amplitude of the effect increases with increasing  $\xi$  and reaches  $\sim 6$   $\mu\text{eV}$  for  $\xi = 0.32$ . For  $\xi = 0.4$  ( $E = 3.05$  meV), the effect is no longer present within the experimental error. This observation is in good accord with the magnitude of the superconducting energy gap  $2\Delta \sim 2.6$  meV extracted from tunneling data [17]. For  $\xi = 0.43$ , there is some indication of an increase in phonon linewidth at low temperatures. This is expected because of the pileup of electronic states above the energy gap. This effect is also responsible for the nonmonotonic temperature dependence of  $\Gamma$  for  $\xi = 0.32$  [Fig. 2(c)]. As  $2\Delta$  approaches the phonon energy  $E$  from below with decreasing temperature,  $\Gamma$  first increases gradually because of the

enhanced density of states above the gap and subsequently plummets sharply below  $T_c$  as  $2\Delta > E$ . It has been shown [14,18] that the jump in phonon linewidth at  $T_c$ , expressed as a fraction of the normal-state linewidth, is equal to the jump in the ultrasound attenuation coefficient at  $T_c$ . This, in turn, can be calculated in BCS theory [18] as  $(\pi/2) \times [1 - 2/(1 + \exp(E/k_B T))] = 1.44$  for  $E = 2.46$  meV and  $T = 4.6$  K (the temperature where  $2\Delta = E$ ), in good agreement with the value  $1.48 \pm 0.1$  determined from Fig. 2(c).

For the more steeply dispersing  $T_2$  phonon along  $(\xi\xi0)$ , the superconductivity-induced phonon linewidth renormalization is much smaller than that of the  $T_1$  phonon, and only upper bounds could be established [Fig. 2(g)]. This is expected on general grounds, because the steep dispersion of this mode implies that the linewidth effects are restricted to wave vectors close to the BZ center. In the  $(\xi\xi\xi)$  direction, where the two transverse phonons are degenerate, we observed a superconductivity-induced linewidth reduction of magnitude similar to that of the  $T_1$  phonon along  $(\xi\xi0)$  [Fig. 2(i)].

In order to compare the experimental results to predictions of *ab initio* calculations, the phonon dispersions and linewidths were calculated in the framework of density functional [19,20] perturbation theory [21] in the local-density approximation. We employed ultrasoft pseudopotentials [22], with scalar-relativistic corrections and a plane-wave basis set [23], with a cutoff energy of 40 Ry. The  $\mathbf{k}$ -space integration was approximated with a  $(12)^3$  Monkhorst-Pack grid [24] using a smearing parameter [25] of 0.06 Ry for the self-consistent cycles and phonon calculations and with a much denser  $(36)^3$  mesh and a Gaussian smearing of 0.04 Ry for the calculation of the linewidths. With these parameters and the numerically optimized lattice parameter of 4.95 Å, the phonon frequencies were converged to 0.1 meV and the linewidths to 0.025  $\mu\text{eV}$ . (If the lattice parameter 4.92 Å determined experimentally at low temperature is used instead, the results are not affected outside these numerical confidence limits.) The calculated phonon frequencies agree with the experimentally determined phonon frequencies [3,4] within the published error bars. For selected  $\mathbf{k}$  points, we recalculated the phonon energies and linewidths using Savrasov's full potential linear muffin-tin orbitals program [1] and found very good agreement.

Figure 3 provides a synopsis of the experimentally determined and numerically calculated electron-phonon linewidths along  $(\xi\xi0)$ . Although the overall agreement is satisfactory, a significant, systematic deviation outside of the experimental error bar is apparent around  $\xi = 0.3$ . A similar deviation was found for the more limited data set along  $(\xi\xi\xi)$ . A possible source of this discrepancy is the spin-orbit coupling, which was not considered in the calculation. The electronic density of states at the Fermi level increases by about 10% when spin-orbit coupling is in-

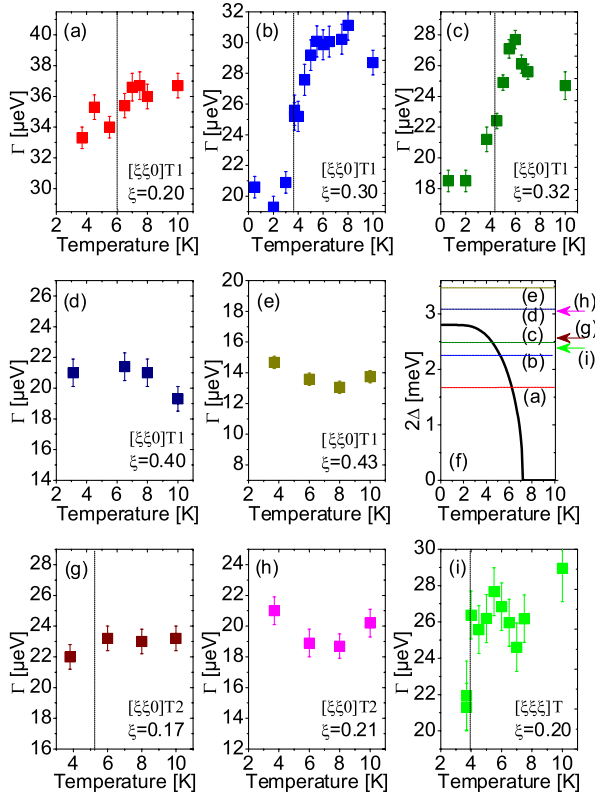


FIG. 2 (color online). (a)–(e) Temperature dependence of the observed NRSE relaxation rate  $\Gamma$  for  $T_1$  phonons along  $(\xi\xi0)$ . (f) Superconducting energy gap from tunneling data [17]. (g),(h)  $\Gamma$  versus temperature for  $T_2$  phonons along  $(\xi\xi0)$  and (i) for a transverse phonon along  $(\xi\xi\xi)$ . The dashed lines in panels (a)–(e),(g),(i) indicate the temperatures at which the superconducting gap opens, according to the data in panel (f).

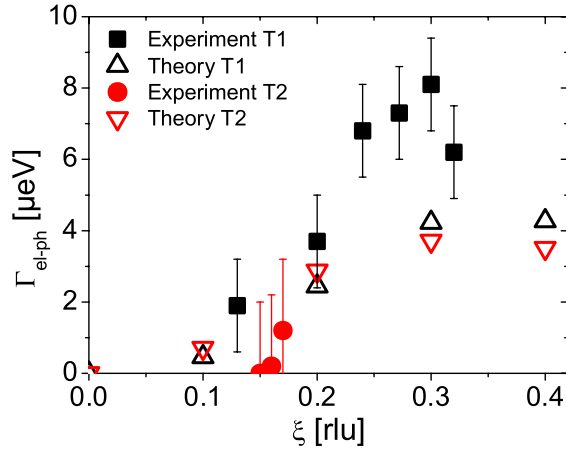


FIG. 3 (color online). Experimentally determined and numerically calculated electron-phonon linewidth of transverse phonons along  $(\xi\xi0)$ . The experimental points were obtained by subtracting the linewidths at 10 K (see Fig. 2) from those at the lowest temperature (0.5 K).

incorporated in the electronic structure calculation. A corresponding increase in the electron-phonon interaction is to be expected. Indeed, Pb is a well-known example in which the agreement between the experimentally determined and theoretically calculated phonon frequencies and total electron-phonon coupling parameter  $\lambda$  is not as good as in the case of other elemental superconductors, such as Al or Nb. In our calculation,  $\lambda$  was computed as 1.27, whereas  $\lambda = 1.55$  was determined by tunneling spectroscopy [17]. Furthermore, the values of  $\lambda$  calculated from first principles range from  $\lambda = 1.2$  (Ref. [26]) to  $\lambda = 1.68$  (Ref. [1]). The experimental results presented here therefore call for further development in the numerical computation of electron-phonon interactions.

In conclusion, we have used neutron resonance spin-echo spectroscopy to determine the electron-phonon contribution to the lifetimes of selected phonons in lead. The results have enabled the first energy- and momentum-resolved test of *ab initio* lattice-dynamical calculations. The energy resolution of the experiment was about 2 orders of magnitude better than that achievable by triple-axis spectroscopy (for a typical triple-axis scan, see the inset in Fig. 1). The method can be applied in a straightforward manner to other elements and compounds that exhibit superconductivity at low temperatures. For nonsuperconducting metals, a rigorous treatment of the resolution function is required to extract the electron-phonon lifetime. The pertinent formalism has already been established [11,15]. The method has recently also been applied to magnetic excitations, opening new perspectives in this field as well [27].

We thank O. K. Andersen, S. P. Bayrakci, and F. Mezei for useful discussions and C. T. Lin for preparing the Pb crystals.

- [1] See, e.g., S. Y. Savrasov, Phys. Rev. B **54**, 16470 (1996); S. Y. Savrasov and D. Y. Savrasov, *ibid.* **54**, 16487 (1996); S. Y. Savrasov, D. Y. Savrasov, and O. K. Andersen, Phys. Rev. Lett. **72**, 372 (1994).
- [2] See, e.g., H. J. Choi, D. Roundy, H. Sun, M. L. Cohen, and S. G. Louie, Nature (London) **418**, 758 (2002); Y. Kong, O. V. Dolgov, O. Jepsen, and O. K. Andersen, Phys. Rev. B **64**, 020501 (2001).
- [3] B. N. Brockhouse, Phys. Rev. **128**, 1099 (1962); R. Stedman, L. Almquist, G. Nilsson, and G. Raunio, *ibid.* **162**, 545 (1967).
- [4] A. Furrer and W. Hälg, Phys. Status Solidi **42**, 821 (1970).
- [5] R. Youngblood, Y. Noda, and G. Shirane, Solid State Commun. **27**, 1433 (1978).
- [6] F. Mezei, *Inelastic Neutron Scattering* (IAEA, Vienna, 1978), p. 125; R. Pynn, J. Phys. E **11**, 1133 (1978).
- [7] T. Keller, B. Keimer, K. Habicht, R. Golub, and F. Mezei, in *Neutron Spin Echo Spectroscopy*, Springer Lecture Notes in Physics Vol. 601, edited by F. Mezei, C. Pappas, and T. Gutberlet (Springer, Heidelberg, 2003), p. 74. Available online at <http://www.fkf.mpg.de/keimer/>.
- [8] F. Mezei, B. Farago, and C. Lartigue, in *Excitations in Two-Dimensional and Three-Dimensional Quantum Fluids*, NATO Advanced Studies Institute, Series B: Physics Vol. 257, edited by A. F. G. Wyatt and H. J. Lauter (Plenum, New York, 1991), p. 119.
- [9] J. Kulda, A. Debernardi, M. Cardona, F. de Geuser, and E. E. Haller, Phys. Rev. B **69**, 045209 (2004).
- [10] R. Golub and R. Gähler, Phys. Lett. A **123**, 43 (1987).
- [11] K. Habicht, R. Golub, F. Mezei, B. Keimer, and T. Keller, Phys. Rev. B **69**, 104301 (2004).
- [12] T. Keller, K. Habicht, H. Klann, M. Ohl, H. Schneider, and B. Keimer, Appl. Phys. A **74**, S332 (2002).
- [13] J. D. Axe and G. Shirane, Phys. Rev. Lett. **30**, 214 (1973); Phys. Rev. B **8**, 1965 (1973).
- [14] S. M. Shapiro, G. Shirane, and J. D. Axe, Phys. Rev. B **12**, 4899 (1975).
- [15] K. Habicht, T. Keller, and R. Golub, J. Appl. Crystallogr. **36**, 1307 (2003).
- [16] P. Aynajian *et al.* (to be published).
- [17] R. F. Gasparovic, B. N. Taylor, and R. K. Eck, Solid State Commun. **4**, 59 (1966).
- [18] V. M. Bobetic, Phys. Rev. **136**, A1535 (1964).
- [19] W. Kohn and L. J. Sham, Phys. Rev. **140**, A1133 (1965).
- [20] P. Hohenberg and W. Kohn, Phys. Rev. **136**, B864 (1964).
- [21] S. Baroni, S. de Gironcoli, A. Dal Corso, and P. Giannozzi, Rev. Mod. Phys. **73**, 515 (2001).
- [22] D. Vanderbilt, Phys. Rev. B **41**, 7892 (1990).
- [23] S. Baroni *et al.*, <http://www.pwscf.org>.
- [24] H. J. Monkhorst and J. D. Pack, Phys. Rev. B **13**, 5188 (1976).
- [25] N. Marzari, D. Vanderbilt, A. De Vita, and M. C. Payne, Phys. Rev. Lett. **82**, 3296 (1999).
- [26] A. Y. Liu and A. A. Quong, Phys. Rev. B **53**, R7575 (1996).
- [27] S. P. Bayrakci, T. Keller, K. Habicht, and B. Keimer, Science (to be published).